



HAL
open science

Complete Complementary Coded Excitation Scheme for SNR Improvement of 2D Sparse Array Ultrasound Imaging

Mohamed Tamraoui, Herve Liebgott, Emmanuel Roux

► **To cite this version:**

Mohamed Tamraoui, Herve Liebgott, Emmanuel Roux. Complete Complementary Coded Excitation Scheme for SNR Improvement of 2D Sparse Array Ultrasound Imaging. IEEE Transactions on Biomedical Engineering, inPress, 10.1109/TBME.2023.3325657 . hal-04321874

HAL Id: hal-04321874

<https://hal.science/hal-04321874>

Submitted on 4 Dec 2023

HAL is a multi-disciplinary open access archive for the deposit and dissemination of scientific research documents, whether they are published or not. The documents may come from teaching and research institutions in France or abroad, or from public or private research centers.

L'archive ouverte pluridisciplinaire **HAL**, est destinée au dépôt et à la diffusion de documents scientifiques de niveau recherche, publiés ou non, émanant des établissements d'enseignement et de recherche français ou étrangers, des laboratoires publics ou privés.

GENERAL INSTRUCTION

- **Authors:** Carefully check the page proofs (and coordinate with all authors); additional changes or updates WILL NOT be accepted after the article is published online/print in its final form. Please check author names and affiliations, funding, as well as the overall article for any errors prior to sending in your author proof corrections. Your article has been peer reviewed, accepted as final, and sent in to IEEE. No text changes have been made to the main part of the article as dictated by the editorial level of service for your publication.
- **Authors:** Authors are required to pay page charges for all pages beyond the first eight pages. For more information please see <https://www.embs.org/tbme/for-authors/>
- **Authors:** If you are unable to pay these charges please let us know.
- **Authors:** We cannot accept new source files as corrections for your article. If possible, please annotate the PDF proof we have sent you with your corrections and upload it via the Author Gateway. Alternatively, you may send us your corrections in list format. You may also upload revised graphics via the Author Gateway.
- **Authors:** Please confirm the name of the corresponding author.

QUERIES

- Q1. Author: Please check and confirm whether the membership detail of the author Mohamed Tamraoui is correct as set.
- Q2. Author: Please confirm or add details for any funding or financial support for the research of this article.
- Q3. Author: Please provide the name of the corresponding author along with city/state, country, postal code and email id.
- Q4. Author: Please provide complete bibliographic details for Ref. [47].
- Q5. Author: Please check whether Ref. [72] is correct as set.
- Q6. Author: Please provide the report number for Ref. [82].

Complete Complementary Coded Excitation Scheme for SNR Improvement of 2D Sparse Array Ultrasound Imaging

Mohamed Tamraoui , Graduate Student Member, IEEE, Hervé Liebgott , Member, IEEE, and Emmanuel Roux , Member, IEEE

Abstract—Driving the numerous elements of 2D matrix arrays for 3D ultrasound imaging is very challenging in terms of cable size, wiring and data rate. The sparse array approach tackles this problem by optimally distributing a reduced number of elements over a 2D aperture while preserving a decent image quality and beam steering capabilities. Unfortunately, reducing the number of elements significantly reduces the active probe footprint reducing as a consequence the sensitivity and at the end the signal-to-noise ratio. Here we propose a new coded excitation scheme based on complete complementary codes to increase the signal-to-noise ratio in 3D ultrasound imaging with sparse arrays. These codes are known for their ideal auto-correlation and cross-correlation properties and have been widely used in Code-Division Multiple Access systems (CDMA). An algorithm for generating such codes is presented as well as the adopted imaging sequence. The proposed method has been compared in simulations to other coded excitation schemes and showed significant increase in the signal-to-noise ratio of sparse arrays with no correlation artifacts and no frame rate reduction. The gain in signal-to-noise ratio compared to the case where no coded excitation is used was around 41.28 dB and the contrast was also improved by 29 dB while the resolution was unchanged.

Index Terms—3D ultrasound, Complete complementary codes, Signal-to-noise ratio, Sparse arrays.

I. INTRODUCTION

WITH three-dimensional ultrasound (3D US) imaging systems a full representation of the 3D anatomy is obtained allowing the clinician to access volumetric information in the observed scene (anatomy, flow,...). Conventionally, these systems use 2D matrix arrays to acquire images of the whole region of interest (ROI). With common sequences, scanning

Manuscript received 4 March 2023; revised 19 July 2023 and 11 September 2023; accepted 9 October 2023. This work was supported by the LABEX PRIMES under Grant ANR-11-LABX-0063 of Université de Lyon, through the Program “Investissements d’Avenir” under Grant ANR-11-IDEX-0007 operated by the French National Research Agency (ANR), performed within the framework of the ANR-20-CE19-0023 SPARTECHUS.

The authors are with the Univ Lyon, INSA-Lyon, Université Lyon 1, CNRS, Inserm, CREATIS UMR, France.

Digital Object Identifier 10.1109/TBME.2023.3325657

the ROI requires an individual control of each element of the array to steer the ultrasound (US) beam in both the elevation and lateral directions. Moreover, to produce images with good lateral resolution and contrast, 2D matrix arrays should be large enough while maintaining the pitch distance between array elements in both directions to one half of the wavelength ($\lambda/2$) [1], [2]. To satisfy these conditions, several thousand small-sized elements are required. For example, to have the same lateral resolution as a 128-element linear array, a 2-D matrix array consisting of $128 \times 128 = 16,384$ elements is needed. Manufacturing an array with several thousands of elements is very complex and costly. As such arrays require as many channels as elements to be driven, it increases the complexity of the electronics controlling the array and the size of the connection cable. Several solutions have been proposed in the literature to overcome these limitations, including row-column addressing (RCA) [3], [4], [5], [6], [7], micro-beamforming [8], [9], [10], [11], and channel multiplexing [12], [13].

The RCA approach considers an $N \times N$ matrix array as an orthogonal set of N rows and N columns. An entire row or column is addressed instead of a single element and one is used for transmit while the other is used for receive. The number of channels required is then reduced to $2N$ instead of N^2 . However, due to element elongation, electronic apodization is not possible as there is no electronic control along the length of each element [14]. Another limitation of RCA is that the array can only scan a ROI of the size of the aperture [15]. Microbeamforming is another solution that aims to reduce the cables and the amount of transferred data from the array to the scanner. Using application-specific integrated circuits (ASIC), signals from a sub-aperture of elements are pre-beamformed directly in the probe and the reduced number of signals are sent through the cable to the scanner. Even though this can allow the control of thousands of elements using a reduced number of channels, the integration of such computational power in the probe requires active cooling which make designing such probes more complex and expensive [16], [17], [18]. Finally, the channel multiplexing techniques, a subset of elements is controlled by the same channel using a multiplexer. These arrays require fewer channels but they suffer from a lack of flexibility to address the elements of the full array, as only a subset of elements can be connected during transmission and reception [19], [20].

In this work we will focus on another solution known as sparse arrays originally described in [21] and recently reviewed in [17].

The sparse arrays approach tackles the limitations associated with the large number of elements of 2D matrix arrays by optimally distributing a reduced number of elements over the aperture of the array, allowing the use of a reduced number of channels. In order to have images with decent quality, the number of elements and the way they are distributed over the aperture must produce a beam pattern with a thin resolution and a low grating-lobes level (GLL) and side-lobes level (SLL). To reduce the GLL, random sparse arrays were introduced [17], [21], [22], [23]. By randomly distributing the elements over the aperture of the array, the constructive interference responsible for the appearance of grating lobes due to periodicity are suppressed, however, the level of secondary lobes is still high which degrades the image quality [21]. Another approach consists in using stochastic methods to optimize the parameters (positions, apodization weights,...) of sparse arrays elements. An energy function based on the beam pattern (limiting GLL and SLL) is used to search for the best configuration among very large number of candidate solutions using a simulated annealing [24], [25], [26], [27], [28] or a genetic algorithm [29], [30], [31]. The obtained arrays are referred to as optimized sparse arrays. Due to the high computational cost required to design optimized sparse arrays, aperiodic arrays have been proposed such as Fermat's spiral array [1], [32]. This array offers very good performances in terms of GLL and inherits rotational symmetry which is ideal for 3D US imaging [17]. After defining the aperture size, the elements distribution of the Fermat's spiral array is only defined by the divergence angle and the total number of elements which make the array ideal for rapid testing and simulations. To reduce even further the GLL while increasing the array sensitivity, a density tapered Fermat's spiral array was proposed in [16] following the works in [33] for antenna design.

The main issue of sparse arrays lies in the need for elements to be small to have a wide directivity, especially when imaging with sequences such as synthetic transmit aperture (STA). This implies that the elements need to emit with low energy and receive with poor sensitivity, which leads in the end to poor signal-to-noise ratio (SNR) [25]. In contrast, large elements produce more energy, but at the cost of a more directional ultrasonic beam. Voxels of the 3D image are then insonified by fewer elements, which reduces the imaging quality (i.e., reduced resolution, contrast). In [34], a sparse array having large elements and large divergence of each element through the use of a lens was introduced. Although, the use of a lens helps improving the divergence of the large elements, it may reduce the SNR as it spreads the acoustical energy over a broader region. In this article, we propose the use of coded excitation in order to increase even further the SNR of sparse arrays.

The SNR is proportional to the amount of transmitted energy. In order to increase the SNR, longer excitation pulses may be used, however, increasing the duration of the pulse affects severely the axial resolution. Coded excitation is another technique usually used to increase the transmitted energy. It was first introduced for radar systems [35] and then applied to ultrasound imaging [36], [37], [38], [39], [40]. This technique consists of

transmitting a long coded pulses to the medium and using a pulse compression step in receive to compress the energy which increase the SNR without affecting resolution. In the literature, various coded excitation schemes have been proposed in medical ultrasound imaging and can be divided into two categories: frequency modulated schemes and phase modulated schemes.

For frequency modulated schemes, the most popular technique is using linear frequency modulated chirps [37], [38], [41], [42], [43], [44], [45]. In a linear chirp, the instantaneous frequency is linearly changing over time allowing a linear sweep of the whole bandwidth of the transducer. The two important parameters of a chirp are its duration and the swept bandwidth. Although chirps have been proved to increase the SNR in ultrasound imaging, this technique suffers from compression sidelobes that can be as high as -13 dB which severely affects the contrast. Mismatched filtering can be used to reduce the compression sidelobes level to around -40 dB at the expense of degrading the axial resolution, but they can still be visible in images because a dynamic range of 60 dB or more is typically used in ultrasound imaging [39]. Different from frequency modulated schemes, phase modulation schemes use binary sequences that are modulated by a pulse at the central frequency of the transducer where a $+1$ corresponds to 0° phase and -1 corresponds to a 180° phase. One of the most popular binary sequences used in medical ultrasound are complementary Golay codes [46], [47], [48], [49], [50], [51]. They consist of a pair of binary sequences that have opposite sidelobes signs which are suppressed by addition of the two compressed signals. However, the pair of sequences are not orthogonal, hence two separate successive transmissions are necessary which lowers the frame rate by a factor of two. Alternatively, spatial coding methods such as Hadamard encoding can be used to increase the SNR. In Hadamard encoding, each element of the array will transmit a pulse weighted by a coefficient from the Hadamard matrix and the received signals are then decoded using the inverse Hadamard matrix [52], [53], [54], [55]. Hadamard encoding was also shown to improve SNR and penetration depth of plane wave imaging without sacrificing the frame-rate [56], [57]. As stated in [58], this type of encoding can also be combined with modulated sequences to further increase the SNR.

Here, we propose a new coded excitation scheme based on *complete complementary codes* (CCC) that increases the SNR of sparse arrays while suppressing the axial sidelobes and maintaining the frame rate unchanged. They were proposed for the first time by Suehiro et al. [59] as an extension of the complementary sets proposed in [60] by reaching the upper bound limit (i.e. $M \leq N$). As it will be further discussed, reaching this upper bound is of particular interest for US imaging as it minimizes the number of required firing. The CCC are often referred to as (M, N, L) -CCC since they are composed of M sets of N binary sequences of length L (i.e., the number of symbols in each sequence is fixed to L). Indeed, these CCC evolved from the Golay codes by, 1) extending the number of sequences in each set (from two to N), and 2) extending the number of sets (from one to M). Thus, they have the advantages that the sum of the auto-correlations of sequences in each set is zero except for zero shift (i.e., delta impulse) and the sum of cross-correlations

of sequences at the same index between any two distinct sets is zero for all shifts. However, the (N, N, N^2) -CCC that they proposed in [59] using N-Shift cross-orthogonal sequences were relatively long (N^2). Interestingly, this construction was later improved by the authors of [61] to construct (M, N, MN) -CCC and (N, N, MN) -CCC with $(M, N \in \mathbb{Z}^+; M \leq N)$. Hence, the required number of symbols in the sequences decreased from N^2 to MN , and it was even further reduced to MN/P with a method for generating $(N, N, MN/P)$ -CCC with $(M, N, P \in \mathbb{Z}^+; M, P \leq N)$ [62]. A review article analyzing the applications of CCC can be found in [63]. For ultrasound imaging, having CCC with shorter sequences offers the possibility to transmit shorter excitation signals. Because of their ideal correlation properties, CCC codes have been extensively applied in Code-Division Multiple Access (CDMA) [64], [65], [66] and Multiple-input multiple-output (MIMO) [67], [68], [69] systems. To the authors knowledge, this work is the first implementation of CCC in medical ultrasound. The authors also believe that they are well adapted for 3D ultrasound imaging with sparse arrays, since they offer the possibility of transmitting with all the elements while using STA beamforming. Although, using conventional focused transmission with sparse arrays gives better SNR than conventional STA, the number of transmissions required to reconstruct the 3D volume is quite large since a focused transmission event is required for each volume line.

II. METHODS

A. Mathematical Framework

Let $\mathbf{s}_1 = (s_1(1), s_1(2), \dots, s_1(L))$ and $\mathbf{s}_2 = (s_2(1), s_2(2), \dots, s_2(L))$ be two sequences of length L , where each symbol can be $+1$ or -1 . The aperiodic correlation function is defined as follows on $\tau \in [1 - L, L - 1]$:

$$R_{\mathbf{s}_1, \mathbf{s}_2}(\tau) = \sum_{t=-\infty}^{+\infty} s_1(t) s_2(t + \tau)^*, \quad (1)$$

where $s_2(t + \tau)^*$ denotes the complex conjugate of $s_2(t + \tau)$. If $\mathbf{s}_1 \neq \mathbf{s}_2$, (1) is called the cross-correlation function of \mathbf{s}_1 and \mathbf{s}_2 and, if $\mathbf{s}_1 = \mathbf{s}_2 = \mathbf{s}$, it is the auto-correlation function denoted by $R_s(\tau)$ and $E_s = R_s(0)$ is called the energy of \mathbf{s} .

Letting $\mathcal{C}_1 = [\mathbf{s}_{1,1}, \mathbf{s}_{1,2}, \dots, \mathbf{s}_{1,N}]$ and $\mathcal{C}_2 = [\mathbf{s}_{2,1}, \mathbf{s}_{2,2}, \dots, \mathbf{s}_{2,N}]$ be two indexed sets of N sequences of length L . Each set is called an (N, L) -sequence set. The correlation between the two (N, L) -sequence set is defined by the following sum:

$$\mathcal{R}_{\mathcal{C}_1, \mathcal{C}_2}(\tau) = \sum_{n=1}^N R_{\mathbf{s}_{1,n}, \mathbf{s}_{2,n}}(\tau). \quad (2)$$

If $\mathcal{C}_1 = \mathcal{C}_2$ then (2) sums the N auto-correlations of sequences of the same set; otherwise, if $\mathcal{C}_1 \neq \mathcal{C}_2$ it sums the N cross-correlations between sequences with the same index n in the two sets.

An (N, L) -Complementary set \mathcal{C}_i is defined as an (N, L) -sequence set whose auto-correlation sum $\mathcal{R}_{\mathcal{C}_i}(\tau)$, is zero except

for the zero shift:

$$\mathcal{R}_{\mathcal{C}_i}(\tau) = E_{\mathcal{C}_i} \delta(\tau) \quad (3)$$

Where $E_{\mathcal{C}_i}$ is the energy of \mathcal{C}_i and $\delta(\tau)$ is the Kronecker's delta function.

A collection of M (N, L) -sequence sets $\mathcal{C} = [\mathcal{C}_1, \mathcal{C}_2, \dots, \mathcal{C}_M]$ represent a (M, N, L) -sequence family with family size M subject to $M \leq N$. A (M, N, L) -sequence family \mathcal{C} is called a *Complete Complementary Code* (CCC) denoted by (M, N, L) -CCC if the two following conditions are satisfied:

1) For every $i \in [1, M]$, we have:

$$\mathcal{R}_{\mathcal{C}_i}(\tau) = E_{\mathcal{C}_i} \delta(\tau) \quad (4)$$

2) For every $i, j \in [1, M], i \neq j$:

$$\mathcal{R}_{\mathcal{C}_i, \mathcal{C}_j}(\tau) = 0 \quad (5)$$

The first condition implies that the sum of the auto-correlations in each sequence set is zero except for the zero shift where it equals $E_{\mathcal{C}_i}$. This means that each sequence set \mathcal{C}_i must be an (N, L) -Complementary set. The second condition implies that, given any two different sets, the sum of the cross-correlations between sequences at the same index is zero at all shifts. In this case, the two sets are then called, cross-complementary sets. Consequently, an (M, N, L) -sequence family is called (M, N, L) -CCC, if all the M sets are (N, L) -Complementary set and any distinct pair of which are cross complementary sets.

For example, if $M = 2, N = 2$ and $L = 4$ the corresponding $(2, 2, 4)$ -CCC $\mathcal{C} = (\mathcal{C}_1, \mathcal{C}_2) = ((\mathbf{s}_{1,1}, \mathbf{s}_{1,2}), (\mathbf{s}_{2,1}, \mathbf{s}_{2,2}))$ is given by:

$$\begin{aligned} \mathbf{s}_{1,1} &= (+ + + -) & \mathbf{s}_{1,2} &= (+ - + +) \\ \mathbf{s}_{2,1} &= (+ + - +) & \mathbf{s}_{2,2} &= (+ - - -) \end{aligned}$$

Where $+$ denotes $+1$ and $-$ denotes -1 . Then the auto-correlation sum of \mathcal{C}_1 and the auto-correlation sum of \mathcal{C}_2 are:

$$\begin{aligned} \mathcal{R}_{\mathcal{C}_1}(\tau) &= R_{\mathbf{s}_{1,1}}(\tau) + R_{\mathbf{s}_{1,2}}(\tau) \\ &= (-1, 0, 1, 4, 1, 0, -1) + (1, 0, -1, 4, -1, 0, 1) \\ &= (0, 0, 0, 8, 0, 0, 0) \end{aligned}$$

$$\begin{aligned} \mathcal{R}_{\mathcal{C}_2}(\tau) &= R_{\mathbf{s}_{2,1}}(\tau) + R_{\mathbf{s}_{2,2}}(\tau) \\ &= (1, 0, -1, 4, -1, 0, 1) + (-1, 0, 1, 4, 1, 0, -1) \\ &= (0, 0, 0, 8, 0, 0, 0) \end{aligned}$$

And the sum of cross-correlation between \mathcal{C}_1 and \mathcal{C}_2 is given by:

$$\begin{aligned} \mathcal{R}_{\mathcal{C}_1, \mathcal{C}_2}(\tau) &= R_{\mathbf{s}_{1,1}, \mathbf{s}_{2,1}}(\tau) + R_{\mathbf{s}_{1,2}, \mathbf{s}_{2,2}}(\tau) \\ &= (-1, 0, 3, 0, 1, 0, 1) + (1, 0, -3, 0, -1, 0, -1) \\ &= (0, 0, 0, 0, 0, 0, 0) \end{aligned}$$

B. Construction of Complete Complementary Codes

Because of their interesting correlation properties, many researchers have tried to develop CCC construction algorithms. Among those methods, we have decided to use the one proposed in [62] to generate an $(N, N, MN/P)$ -CCC because it allows generating CCC with short sequences length.

As it was proposed in [62], *unitary matrices* are used in order to generate a $(N, N, MN/P)$ -CCC. An $N \times N$ matrix U_N is called *unitary* if it satisfies $U_N U_N^t = U_N^t U_N = I_N$, where I_N denotes the $N \times N$ identity matrix. A good candidate for the *unitary matrix* is the *Hadamard matrix* which is the one used in this article. Additionally, P and M values must be chosen so that P divide into N , and M divide into N/P . After choosing the M , N and P values for the desired $(N, N, MN/P)$ -CCC, the construction method is divided into four steps :

- 1) We split column-wise a *Hadamard matrix* of size $N/P \times N/P$ into $N/(MP)$ matrices $A_1, A_2, \dots, A_{N/(MP)}$ of size $N/P \times M$ (A_i is the i -th block of M columns of A).
- 2) Then, a matrix \mathcal{D} of size $N^2/P^2 \times MN/P$ can be constructed as follows :

$$\mathcal{D} = \begin{bmatrix} (B \otimes C) \cdot \text{Diag}(\text{Vec}(A_1)) \\ (B \otimes C) \cdot \text{Diag}(\text{Vec}(A_2)) \\ \vdots \\ (B \otimes C) \cdot \text{Diag}(\text{Vec}(A_{N/MP})) \end{bmatrix} \quad (6)$$

with, B and C two *Hadamard matrices* of respective size $M \times M$ and $N/P \times N/P$ and with, \otimes the Kronecker product, the matrix multiplication, Diag the diagonal operator and Vec the vectorization operator.

- 3) We construct a new matrix \mathcal{H} of size $N/P \times MN^2/P^2$ by concatenating the rows of the i -th block of N/P rows of \mathcal{D} to form a single row \mathcal{H}_i of \mathcal{H} :

$$\mathcal{H} = \begin{bmatrix} \mathcal{H}_1 \\ \mathcal{H}_2 \\ \vdots \\ \mathcal{H}_{N/P} \end{bmatrix}, \mathcal{H}_i = [d_{1+r_i}, d_{2+r_i}, \dots, d_{N/P+r_i}] \quad (7)$$

where an indexed d is a single row of \mathcal{D} and $r_i = (i - 1)N/P$ with $i \in [1, N/P]$.

- 4) The final $(N, N, MN/P)$ -CCC matrix \mathcal{C} of size $N \times MN^2/P$ is obtained with the Kronecker product of a *Hadamard matrix* E of size $P \times P$ with matrix \mathcal{H} :

$$\mathcal{C} = E \otimes \mathcal{H} = \begin{bmatrix} \mathcal{C}_1 \\ \mathcal{C}_2 \\ \vdots \\ \mathcal{C}_N \end{bmatrix} = \begin{bmatrix} s_{1,1} & s_{1,2} & \dots & s_{1,N} \\ s_{2,1} & s_{2,2} & \dots & s_{2,N} \\ \cdot & \cdot & \dots & \cdot \\ s_{N,1} & s_{N,2} & \dots & s_{N,N} \end{bmatrix} \quad (8)$$

Where each of the N rows of the \mathcal{C} matrix corresponds to a set of N sequences and each entry $s_{i,j}$ is a sequence of length MN/P . The code used to generate CCC, including test functions was implemented in MATLAB and is provided publicly through a github repository (<https://github.com/Tamraoui/CompleteComplementaryCodes>).

C. Imaging Method

To increase the SNR of 3D sparse arrays, a CCC excitation scheme is applied to the STA imaging sequence. Unlike Conventional STA, all the elements transmit simultaneously N times. Instead of transmitting the same short pulse, each i -th element transmits the sequence $s_{i,j}$ during the j -th transmission event. So, in this coded excitation scheme, all the elements transmit a different sequence picked from the $(N, N, MN/P)$ -CCC matrix \mathcal{C} at each transmission event. After the N transmissions and thanks to the ideal auto-correlation and cross-correlation properties of CCC, the received signals are then decoded without any mutual interference. Hence, we recover the full STA dataset as would yield the standard STA approach under the assumption of an ideal, linear, propagation medium, but with much higher SNR.

More precisely, (8) shows that \mathcal{C} is composed of N sequence sets \mathcal{C}_i with $i = (1, 2, \dots, N)$. And each set \mathcal{C}_i contains N binary sequences $s_{i,j}$ with $j = (1, 2, \dots, N)$. Each binary sequence has length MN/P . In the proposed coded excitation scheme each of the N transducer elements will be assigned a sequence set \mathcal{C}_i , thus element 1 is assigned the set \mathcal{C}_1 , element 2 is assigned the set \mathcal{C}_2 and so on. Since each set is composed of N sequences, to make profit of the ideal auto-correlation and cross-correlation properties of CCC, all the sequences need to be transmitted requiring N transmit events to be made. In each transmit event, all the elements are activated simultaneously and each one of them will transmit the sequence $s_{i,j}$ from the assigned set \mathcal{C}_i .

As depicted in Fig. 1, the transmission scheme works as follows: in transmit event 1, element 1 transmits the sequence $s_{1,1}$, element 2 transmits the sequence $s_{2,1}$ and element N transmits the sequence $s_{N,1}$. In the second transmit event, element 1 transmits the sequence $s_{1,2}$, element 2 transmits the sequence $s_{2,2}$ and element N transmits the sequence $s_{N,2}$. And the transmit events continue until the last transmit event during which element 1 transmits the sequence $s_{1,N}$, element 2 transmits the sequence $s_{2,N}$ and element N transmits the sequence $s_{N,N}$.

In practice, the binary $(N, N, MN/P)$ -CCC sequences can not be used directly to drive the transducer because the spectrum of a binary code is much wider than the transducer bandwidth. Instead of a direct sequence transmission, a modulation is applied to make good use of the transducer bandwidth and maximize the transmitted energy: before transmission, a binary phase shift keying (BPSK) modulation is used to make each sequence bandwidth match the bandwidth of the transducer. In (BPSK) each code bit is modulated with a pulse at the central frequency of the transducer with an integer number of cycles and a phase of 0° for a $+1$ bit and a phase of 180° for a -1 bit. The modulation and its effect on the spectrum of a 16-bit binary $(1, -1, 1, 1, 1, -1, -1, -1, 1, -1, 1, 1, -1, 1, 1, 1)$ sequence is illustrated in Fig. 2. Each bit is modulated by a 1 cycle sine wave at a frequency of 7 MHz.

In order to recover the STA dataset as if the elements had transmitted one at a time, the received RF signals (recall that all elements are receiving after each transmission events) need to be decoded. In order to recover the data of the i -th element, the RF signals received after each simultaneous transmit event

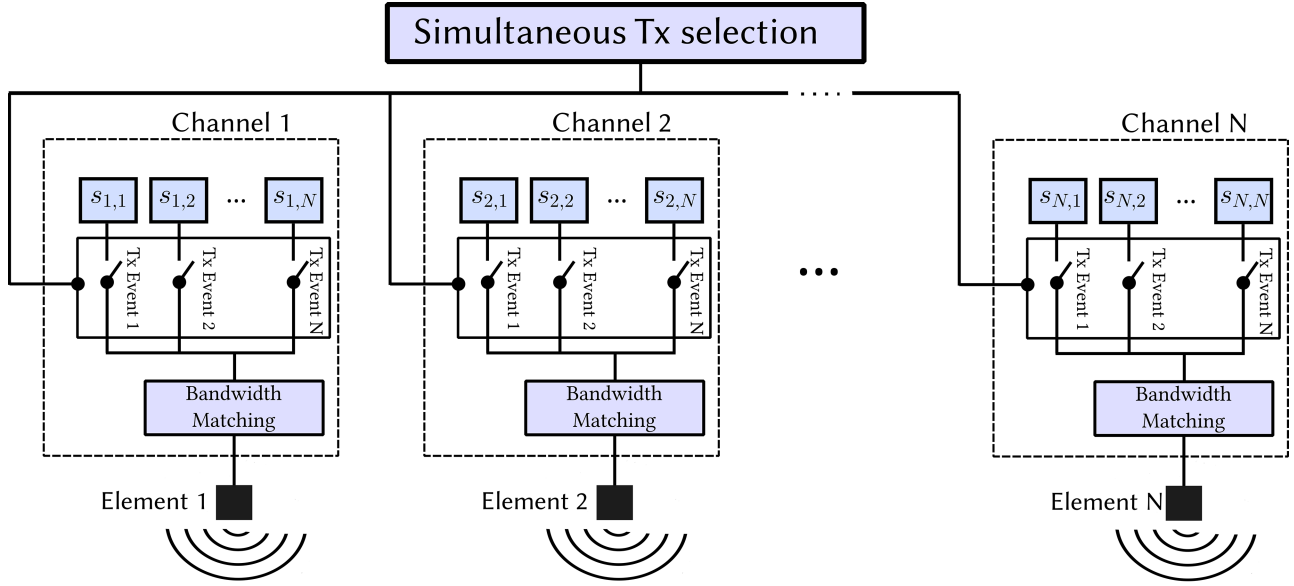


Fig. 1. Principal of STA imaging transmission scheme using $(N, N, MN/P)$ -CCC.

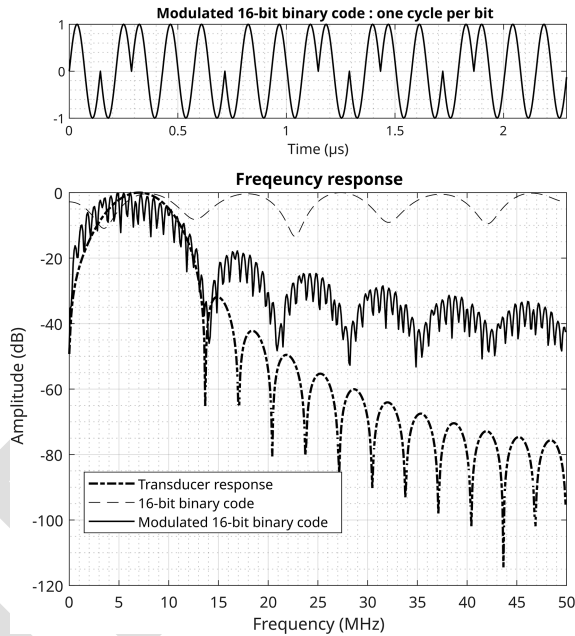


Fig. 2. Modulation of a 16-bit binary code (top) and its corresponding frequency response plotted against the response of the transducer and an unmodulated binary code (bottom).

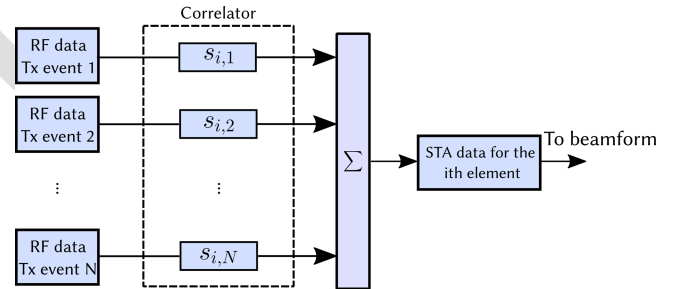


Fig. 3. Decoding block of the received RF data to retrieve the STA dataset.

from the i -th transmitter are kept with higher SNR and the RF signals from all the other transmitters are eliminated when ideal, linear, propagation medium is considered. 375
376
377

III. RESULTS 378

A. Simulation Setup 379

For simulation, a 256 elements Fermat's spiral array with a golden divergence angle and a 50% Tukey window density tapering was constructed following the methods proposed in [16]. 380
381
382
It is illustrated in Fig. 4. We considered a central frequency of 7 MHz with a -6 dB fractional bandwidth of 96% for each transducer element and an aperture of 15 mm diameter with square elements of size 1.5λ , with λ being the wavelength. 383
384
A summary of the parameters of the array are listed in Table I. Simulations were carried out using the Field II ultrasound simulation software [70], [71]. Frequency dependent attenuation was not accounted for in the simulations in order to test the codes in ideal propagations conditions and to verify the theoretically expected SNR gains. As mentioned in [72], frequency dependent 385
386
387
388
389
390
391
392

366 are correlated with the sequence $s_{i,j}$ that was transmitted by the
367 i -th element in that specific event (the j -th) and then summed
368 together. Fig. 3 illustrates the decoding process for the i -th element.
369 In other words, the received RF signals after each transmit
370 event are correlated with the sequences of the set \mathcal{C}_i assigned to
371 the i -th element. And since the sum of the auto-correlations of
372 sequences in same set is a delta function (4) and the sum of the
373 cross-correlations between each two sets is zero (5), summing
374 the correlated RF signals will ensure that only the RF signals

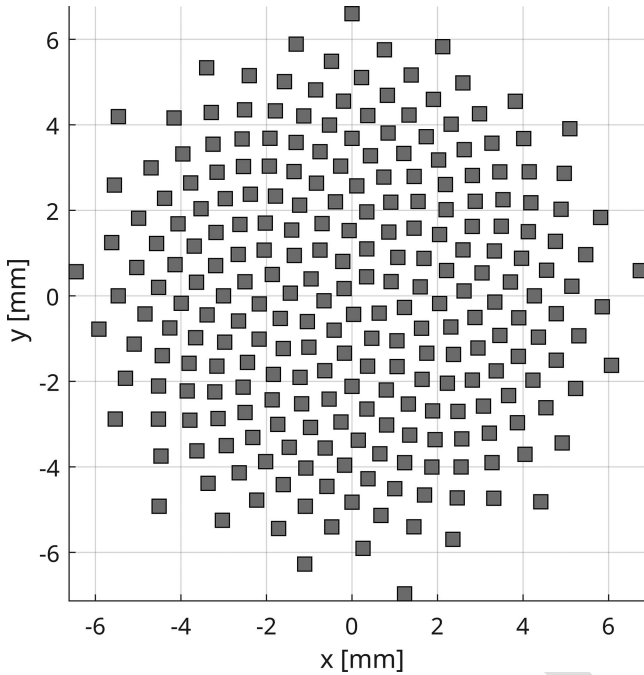


Fig. 4. 256 elements spiral array used in the simulations.

TABLE I
SPARSE ARRAY PARAMETERS

Parameter	Value	Unit
Central frequency	7	MHz
Aperture size	15	mm
Number of elements	256	-
Element shape	square	-
Element size	1.5	wavelength

attenuation affects the received signals and the output of the matched filter does not correspond to the autocorrelation of the coded sequence which in turns reduces the SNR gains. Even if not tested in this study, many approaches have been considered in order to reduce the effect of attenuation during decoding [44], [73], [74], [75]. The performance of the proposed CCC STA in increasing the SNR was compared with the Hadamard STA, Chirp STA, Golay STA, combined Hadamard-Chirp STA and combined Hadamard-Golay STA. An additive white Gaussian noise was generated according to the bandwidth of the transducer using a pass-band filter and added to Conventional STA RF data. The same type and level of noise was also added to the RF data simulated with the coded excitation techniques before decoding and beamforming.

For a 256 elements spiral array, an (256, 256, 64)-CCC was generated. The generated CCC contains 256 sets, each one is composed of 256 binary sequences. Each element of the array is assigned a set of 256 sequences. To make profit of the ideal auto-correlation and cross-correlation properties of CCC during decoding, all the sequences need to be transmitted, therefore, 256 transmissions are required. Binary sequences of lengths 64 bits were used during the simulations. The sequences were modulated by a 1 cycle, Hanning weighted sine wave at 7 MHz

with a sampling frequency of 100 MHz giving excitation signals of duration 9 μ s.

Conventional STA was simulated using a short pulse of 0.14 μ s. The pulse is a 1 cycle, Hanning weighted sine wave at 7 MHz. For Hadamard STA a 256 order *Hadamard matrix* is required. In each transmission, elements are excited with the same short pulse used for Conventional STA but weighted by a coefficient from the corresponding row of the *Hadamard matrix*. The inverse of the *Hadamard matrix* is used for decoding. For Chirp STA, a chirp with a duration of 9 μ s tapered by a Tukey window was used. The swept bandwidth of the chirp was chosen as 7 MHz which is slightly larger than the transducer's bandwidth (6.75 MHz) as suggested by [39], in order to minimize the effect of the convolution between the transducer impulse response and the excitation signal. The compression was done using a mismatched filter with Hanning window to reduce side-lobes level. For Golay STA, a complementary Golay pair of length 64 bits was generated which will give two complementary excitation signals of same duration (9 μ s) after bandwidth matching. The same parameters of the Hadamard STA, Chirp STA and Golay STA codes were used for combined Hadamard-Chirp STA and Hadamard-Golay STA.

The performance of the coded excitation methods was quantified using the *peak signal to noise ratio* (PSNR) and the *contrast ratio* (CR). To assess the PSNR, a *point spread functions* (PSFs) phantom composed of 5 scatterers was simulated. The scatterers have been axially placed in front of the transducer starting from 20 mm to 60 mm by a step of 10 mm between each two scatterers Fig. 5(a). The PSNR was then calculated on the beamformed images using the following formula [53]:

$$(PSNR)_{dB} = 20 \log_{10} \left(\frac{\max(S_{scat})}{\sigma_{noise}} \right) \quad (9)$$

Where $\max(S_{scat})$ is the peak signal of the scatterer and σ_{noise} is the root mean square of the noise at the same depth as the scatterer.

To assess the CR, a 3D phantom of size 15 \times 15 \times 10 mm (*xyz*) containing an anechoic spherical cyst placed at depth of 35 mm with a diameter of 8 mm was used. For computational limitation, to imitate a real 3D phantom only XZ, YZ and XY planes were generated with randomly distributed scatterers Fig. 8(a). In each plane, grating lobes coming from scatterers placed in the other planes will be visible inside the anechoic inclusion. In order to have a fully developed speckle 10 scatterers per resolution cell was chosen with Gaussian distributed amplitudes. The contrast was then calculated as follows :

$$(CR)_{dB} = 20 \log_{10} \left(\frac{\mu_{cyst}}{\mu_{bck}} \right) \quad (10)$$

Where μ_{cyst} and μ_{bck} are the mean image intensities respectively inside the cyst and in the surrounding background.

B. PSFs Phantom Results

The simulated PSFs images obtained with Conventional STA and the different coded excitation techniques are shown in Fig. 5. The 5 scatterers have been axially placed in front of the transducer starting from 20 mm to 60 mm by a step of 10 mm

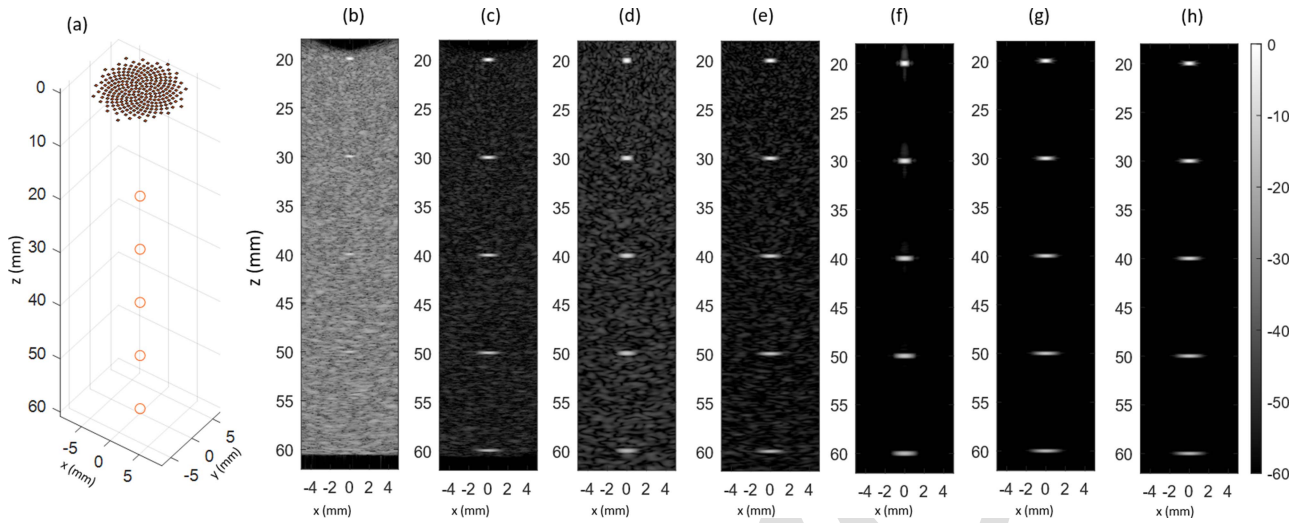


Fig. 5. Simulated beamformed PSFs (a) images obtained with (b) Conventional STA, (c) Hadamard STA, (d) Chirp STA, (e) Golay STA, (f) Hadamard-Chirp STA, (g) Hadamard-Golay STA, (h) proposed CCC STA.

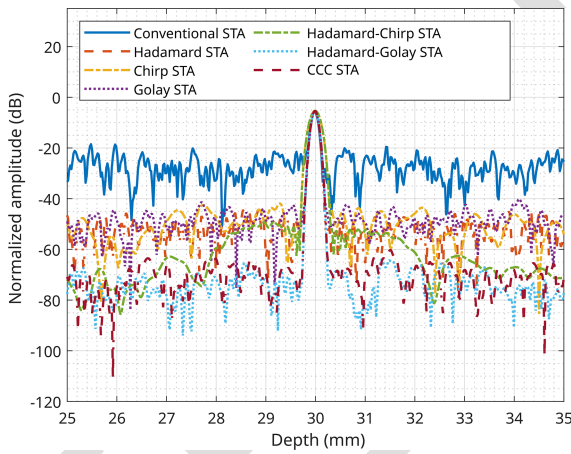


Fig. 6. Axial line plots of the scatterer at the depth of 30 mm for the different excitation schemes.

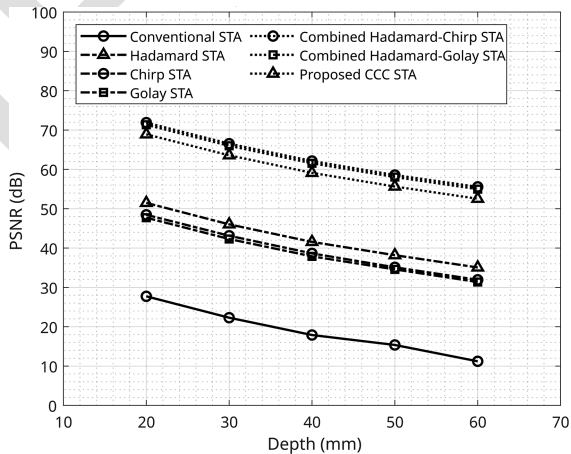


Fig. 7. PSNR for the compared excitation schemes as a function of depth of the 5 scatterers.

between each two scatterers. All of the images have a dynamic range of -60 dB and were simulated with an excitation signal of $9\mu\text{s}$ duration for the coded excitation schemes and a noise condition of -45 dB SNR on the RF data. This noise condition does not seem realistic, especially that only one element is used during each transmit event in the case of Conventional STA, but it was chosen to make sure that the noise will be visible in the images to demonstrate the ability of CCC STA to increase the SNR compared to the other coded excitation methods.

The image produced by the Conventional STA is very noisy which makes it difficult to differentiate the scatterers from the noise because of the low SNR of sparse arrays. Compared to the Conventional STA image, it is visually clear that all the coded excitation schemes lowered the noise in the images, confirming the ability of coded excitation to improve the SNR. In spite of a strong noise reduction, the background remains slightly noisy in the cases of a first group made of those three methods: Hadamard STA, Chirp STA and (to a lower extent) Golay STA. On the contrary, a higher SNR improvement is achieved in the case of this second group of methods (Hadamard-Chirp STA, Hadamard-Golay STA, CCC STA): the noise seems to be completely removed from the images. As expected, in Fig. 5(f), axial side lobes are visible especially around the scatterers close to the transducer, however, they are less visible around scatterers at greater distance due to depth-dependent attenuation, but they are still around -40 dB compared to the amplitude of the main lobe.

To further demonstrate the results, Fig. 6 shows an axial line plot over the scatterer placed at 30 mm. As previously, the compared coded excitation techniques cluster into two groups: with the first group (Hadamard STA, Chirp STA, Golay STA), the background noise level is about 20 dB below to the one of Conventional STA. With the second group of methods (Hadamard-Chirp STA, Hadamard-Golay STA, CCC STA),

466
467
468
469
470
471
472
473
474
475
476
477
478
479
480
481
482
483
484
485
486
487
488
489
490
491
492
493
494
495
496
497
498
499
500

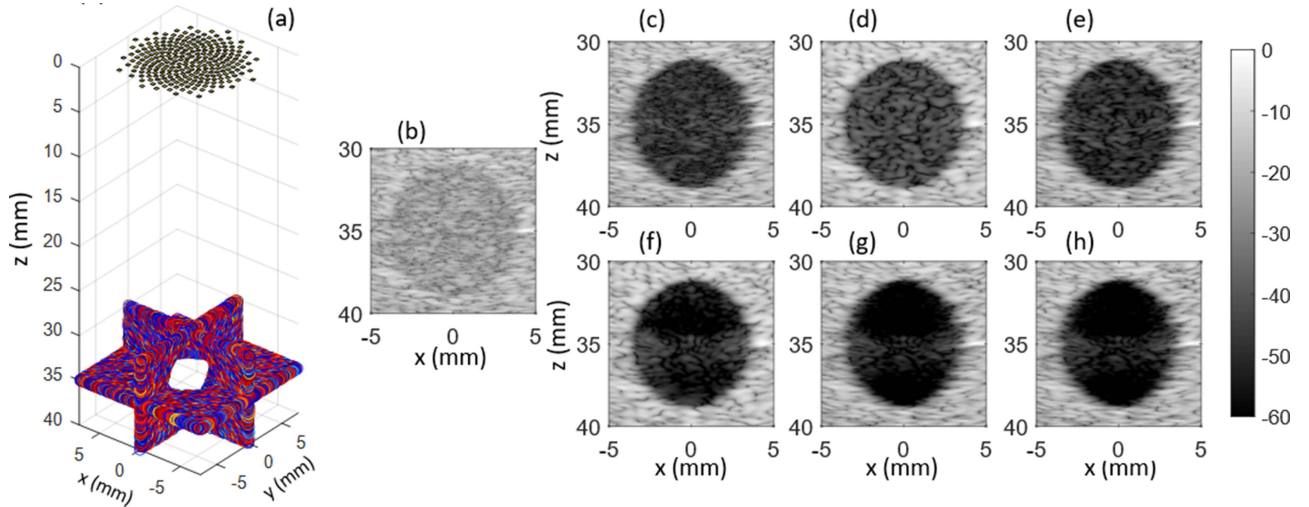


Fig. 8. Simulated beamformed cyst phantom (a) images obtained with (b) Conventional STA (CR = -6 dB), (c) Hadamard STA (CR = -28.52 dB), (d) Chirp STA (CR = -27.60 dB), (e) Golay STA (CR = -30.11 dB), (f) Hadamard-Chirp STA (CR = -35.77 dB), (g) Hadamard-Golay STA (CR = -35.90 dB), (h) proposed CCC STA (CR = -35.88 dB).

TABLE II

COMPARISON OF THE -6 dB AXIAL RESOLUTION COMPUTED ON THE SCATTERER AT DEPTH 30 mm

	-6 dB Axial resolution
Conventional STA	0.16
Hadamard STA	0.16
Chirp STA	0.26
Golay STA	0.17
Hadamard-Chirp STA	0.26
Hadamard-Golay STA	0.17
CCC STA	0.17

Values are given in mm.

TABLE III

COMPARISON OF THE SNR GAINS OBTAINED (ON PSFs PHANTOM) WITH VARIOUS DURATION OF THE EXCITATION SIGNALS

Duration	$0.14\mu s$	$9\mu s$	Theoretical gain($9\mu s$)
Bits	-	64	-
Hadamard STA	23.73	24	-
Chirp STA	-	20.83	17.39
Golay STA	-	20.01	21.07
Hadamard-Chirp STA	-	44.23	41.91
Hadamard-Golay STA	-	43.71	45.15
CCC STA	-	41.28	42.14

Values are given in dB.

501 an improvement of about 40 dB was achieved. Table II
 502 provides a comparison of FWHM axial resolution calculated on
 503 the 30 mm placed scatterer. In accordance with what can be
 504 visually seen in Fig. 6, the table shows that compared to
 505 Conventional STA where an axial resolution of 0.16 mm was
 506 obtained, Hadamard STA, Golay STA, Hadamard-Golay STA
 507 and CCC STA coded methods did not affect the axial resolution
 508 while a degradation has been observed in the case of Chirp STA
 509 and Hadamard-Chirp STA where a value of 0.26 mm was
 510 obtained.

511 Furthermore, Fig. 7 shows a comparison of the PSNRs com-
 512 puted on each of the 5 axially placed scatterers displayed in
 513 the images of Fig. 5. When comparing to Conventional STA,
 514 the gain in SNR is constant as a function of depth regard-
 515 less of the method used since frequency dependent attenua-
 516 tion was not considered. Again, we distinguish two groups of
 517 performing methods. On the one hand, Hadamard STA shows
 518 a gain of around 24 dB, and both Chirp STA and Golay STA
 519 yield around 21 dB of SNR gain. On the other hand, the
 520 Hadamard-Chirp STA and Hadamard-Golay STA reaches an
 521 SNR gain of 44.23 dB and 43.71 dB respectively and our
 522 proposed CCC STA achieves a slightly lower performance of
 523 41.28 dB SNR gain. In addition, Table III provides a summary
 524 of the SNR gains obtained by all the compared methods along

with the theoretical expected gains. We discuss these results in
 Section IV.

C. Cyst Phantom Results

527 To assess the effect of coded excitation on the contrast,
 528 B-mode images of 3D cyst phantom were simulated with
 529 the different methods under a -25 dB SNR noise condition
 530 on the RF data. We have chosen a different SNR condition
 531 for the cyst phantom compared to the PSFs phantom in order
 532 for the anechoic inclusion to be visible. The energy coming
 533 from all the scatterers of the cysts is very large compared to
 534 the PSFs phantom where we only have 5 scatterers and if the
 535 same SNR condition was chosen the quantity of noise would
 536 be important making the anechoic inclusion invisible. In Fig. 8,
 537 since the spiral array inherits rotational symmetry, slices in the
 538 XZ plane from the full 3D reconstructed volume are shown with
 539 a dynamic range of -60 dB. It can be observed that the quality
 540 of the reconstructed images improves by using coded excitation
 541 compared to Conventional STA. The Conventional STA image
 542 is highly degraded by noise making it hard to differentiate
 543 the cyst from the background. In the case of Hadamard STA,
 544 Chirp STA and Golay STA, the quality of the images has been
 545

improved but artifacts are still present inside the anechoic inclusion because the noise has not been completely removed. However, the proposed CCC STA, Hadamard-Chirp STA and Hadamard-Golay STA achieve better images quality and the level of artifacts inside the anechoic inclusion has been highly reduced.

These qualitative results are validated quantitatively by the computed CR values reported in Fig. 8. Conventional STA have the worst CR value compared to the other methods with a value of -6 dB. Hadamard STA, Chirp STA and Golay STA achieve CR values of -28.52 dB, -27.60 dB and -30.11 dB, respectively. Thanks to the high SNR gains, the proposed CCC STA, Hadamard-Chirp STA and Hadamard-Golay STA present a similar CR with a value around -35 dB.

IV. DISCUSSION

To our knowledge, this study is the first use of complete complementary codes to increase SNR for sparse array 3D ultrasound imaging. We compared with five well-known coded excitations schemes (Hadamard STA, Chirp STA, Golay STA and a combined Hadamard-Chirp STA and Hadamard-Golay STA).

Great care was taken to ensure a fair comparison between the different techniques by, 1) using excitation signals with the same duration and, 2) adding the same noise level to the received RF signals before decoding. However, for Conventional STA and Hadamard STA short pulses were used (Table II) since those methods have no pulse compression step in reception. To assess the SNR improvement using coded excitation, the noise was generated within the array bandwidth using a pass-band filter to obtain after filtering, a -45 dB SNR on the Conventional STA RF signals, for PSFs phantom simulations and, -25 dB, for cyst phantom simulations. Then, the same noise was added to the RF signals of the other coded excitation techniques before decoding.

Theoretically, when comparing Conventional STA with Hadamard STA, an SNR gain of $10 \log_{10}(N) = 10 \log_{10}(256) = 24$ dB is expected, where N is the number of transmissions. The simulation results from Table III and Fig. 7 shows a gain around 23.7 dB which is close to the theoretical value. The same trend was also observed in the case of Chirp STA, the expected SNR gain corresponds to the difference between the Time-Bandwidth product of the Chirp and the same computation for the short pulse : $10(\log_{10}(9 * 6.5) - \log_{10}(0.14 * 7.7)) = 17.39$ dB. However, from Table III it can be observed that the SNR gain for Chirp STA is around 20.8 dB which is 3 dB more than what was expected. This is due to the use of a mismatched filter in compression instead of a matched filter as was also observed in [45]. When using Golay STA an SNR gain of 20 dB is obtained that matches the theoretical expected value. In fact, the expected theoretical gain in SNR when using Golay codes is $10 \log_{10}(N.L) = 10 \log_{10}(2 * 64) = 21.07$ dB, where $N = 2$ is the number of transmissions required to transmit the two Golay complementary codes, and $L = 64$ is the length of each code. For the Hadamard-Chirp STA, Hadamard-Golay STA, and our proposed CCC STA methods, instead of using only one element in each transmission event, all the elements are used to

transmit a long duration waveform: this increases the acoustic energy delivered to the medium which explains the high SNR gains observed for this group of methods (Table III and Fig. 7). Theoretically, using the $(N, N, MN/P)$ -CCC sequences, an SNR gain of $10 \log_{10}(N.L) = 10 \log_{10}(256 * 64) = 42.14$ dB is expected, where $N = 256$ is the number of transmission and $L = 64$ is length of the binary sequences. This theoretical value is close to the 41.28 dB gain reported in Table III. Combined Hadamard-Golay STA gives a SNR gain of 43.7 dB which is around 3 dB greater than the proposed CCC STA because the transmission events are doubled: this comes at the cost of frame rate divided by two. In a nutshell, the presented results demonstrates the SNR improvement offered by the simultaneous transmission of all the elements during each transmission event.

Moreover, one of the limitations of using Chirps in coded excitation is the degradation of the axial resolution and the presence of axial side-lobes. Usually the compressed chirps have axial side-lobes that severely affect the contrast, which can be as high as -13 dB. The axial side-lobes level was reduced by using a tapered chirp and a mismatched filter in compression at the price of degrading the axial resolution as shown in Fig. 6 and Table II for Chirp STA and Hadamard-Chirp STA. The axial side-lobes have been reduced to around -40 dB but the main-lobe is broader compared to the other techniques. Even if the axial side-lobes are reduced their presence is still observed in the B-mode cyst images as shown in Figs. 5(f) and 8(f). The artifacts inside the anechoic inclusion are more important in the case of Chirp STA and Combined Hadamard-Chirp STA especially in the interface with background speckle. However, in the proposed CCC STA, the axial resolution is not affected since each bit of the sequences was modulated by a 1 cycle sine pulse which matches with the short pulse used for Conventional STA and Hadamard STA. The same thing can be said for Golay STA and Hadamard-Golay STA. Thanks to the ideal auto-correlation and cross-correlation properties of the binary $(N, N, MN/P)$ -CCC sequences that we used and the ideal, linear, propagation medium consideration, no axial side lobes are present as can be seen in Figs. 5(h) and 8(h). Although they are not visible in Fig. 5 especially in the images where the noise has been reduced since they appear outside the beam-formed region, lateral grating lobes were not affected by coded excitation since they highly depend on the distribution of the sparse array elements. This can be confirmed in Fig. 8(f), (g), and (h), where grating lobes coming from scatterers in the planes YZ and XY are visible in the middle of the anechoic inclusion. The artifacts distribution shows no significant difference between Hadamard-Chirp STA, Hadamard-Golay STA and CCC STA.

Furthermore, the disadvantage of using Golay codes is that 512 transmission events are required rather than 256. In fact, Golay STA and combined Hadamard-Golay STA uses two complementary codes that need to be transmitted one after another by each element of the array. This is because the two codes are not orthogonal, so in order to avoid cross-correlation interference two separate transmissions are required. Transmitting the two codes separately helps yielding a better SNR but the frame rate is divided by two compared to Conventional STA. With

the proposed CCC STA, each element of the array is assigned a set of sequences from the $(N, N, MN/P)$ -CCC used. Because the sets are cross complementary, simultaneous transmissions of the sequences are possible without cross-correlation interference during decoding. This requires only 256 transmissions to be made to increase the SNR while keeping the frame rate unchanged.

The main goal of this work was to introduce the theory of the CCC STA and verify that the improvement of the SNR with the 2D sparse arrays matches with the theoretical expected value and compare it with other coded excitation schemes. The proposed method gives very similar SNR gains compared to combined Hadamard-Chirp STA and combined Hadamard-Golay STA with the advantages of a better resolution as reported in Table II and the absence of correlation artifacts over Hadamard-Chirp STA and the advantage of maintaining the same frame rate as Conventional STA over Hadamard-Golay STA.

When performing 3D US imaging with sparse arrays using conventional focused transmissions, multiple elements are used to transmit and steer a focused beam at a certain depth. Therefore, they provide a higher SNR than Conventional STA where only one element is used during each transmission. This explains the poor image quality in Figs. 5(b) and 8(b). However, unlike Conventional STA, they require a very large number of transmissions in order to reconstruct the full 3D volume since a focused transmission is required for each scanline (e.g. 100×100 scanlines). Additionally, the 3D images produced by conventional focused transmission methods have an optimal quality only at the depth of the transmit focus and degrades out of this depth. This highlights the advantages of using CCC with sparse arrays as they allow simultaneous transmission with all the elements which highly increases the SNR and produces 3D images focused in every voxel, while keeping the number of transmissions to be the same as in Conventional STA.

Additionally, we have compared these three methods in terms of SNR gain relatively to the transmitted energy. The other methods were excluded from this comparison since they offer less SNR gains. The metric is simply the PSNR gain divided by the integral of the squared excitation signal (energy). Fig. 9 shows the values of PSNR by transmitted signal energy (dB/J) as a function of depth with a $9 \mu\text{s}$ excitation duration. It can be seen that compared to combined Hadamard-Chirp STA and combined Hadamard-Golay STA the proposed CCC STA allows more SNR gain with less transmitted signal power.

As with any coded excitation technique, one must take care of the sequence length used in CCC STA. In fact, from one side using long sequences increases the energy transmitted to the medium which in turn increases the SNR gain. However, on the other side, the problem of increasing the sequence length is that during transmission the transducer cannot receive echoes until all the bits of the sequence have been transmitted, increasing the dead zone area. Thanks to the $(N, N, MN/P)$ -CCC codes one can construct sequences with a flexible length to adjust the ideally short dead zone. In this article, CCC of length 64 bits with a dead zone area of 7 mm were used, but shorter lengths are possible as long as M and P values are chosen correctly so that P divide into N, and M divide into N/P in

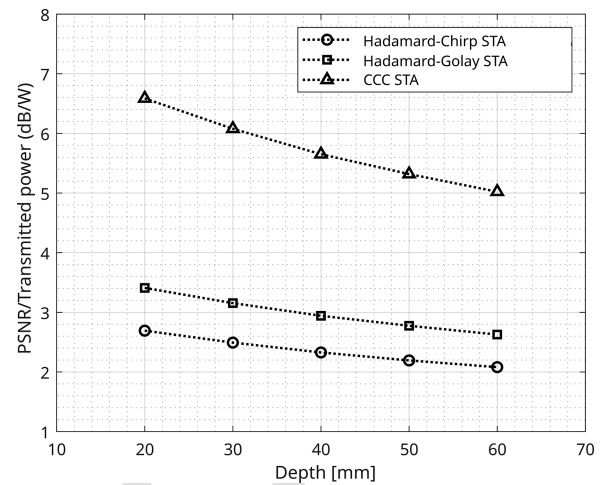


Fig. 9. Comparison between the proposed CCC STA, Hadamard-Chirp STA and Hadamard-Golay STA in terms of PSNR gain per transmitted signal power.

order to obtain the desired MN/P length. Moreover, for a fixed number of bits, the sequences can be made longer or shorter by adjusting the number of cycles (e.g. half cycle, two cycles,...) in the modulating pulse without affecting the ideal correlation properties of the codes. Increasing the number of cycles will produce more SNR gain since the code's frequency response will better fit in the transducer bandwidth allowing more energy to be transferred, but at the expense of reducing a little bit the axial resolution.

As commonly known, the transducer's bandwidth plays a significant role in the implementation and effectiveness of coded excitation techniques in ultrasound imaging [76]. Sparse arrays based on PZT have been developed in previous studies but they suffer from a relatively low bandwidth. In [77], two prototype 2D spiral arrays were designed at center frequencies 2.5 MHz (low-frequency) and 5 MHz (high-frequency) based piezoelectric material built directly on printed circuit boards (PZT-on-PCB). The measured -3 dB one-way bandwidth of the two probes were 0.6 ± 0.3 MHz ($26\% \pm 13\%$) and 1.6 ± 0.6 MHz ($32\% \pm 11\%$) respectively. While these bandwidths are sufficient for fundamental mode imaging, they are too low for contrast imaging at higher harmonics and are not optimal for coded excitation. The poor impedance matching between the PZT and the PCB resulted in significant reflections within the PZT, thereby reducing the bandwidth of the probes. Currently, we are collaborating with an ultrasound probe manufacturer for the development of a PZT based spiral sparse array with a 60% fractional bandwidth which allows more energy to be transmitted when using CCC. Additionally, as proposed in [76], bit elongation can be used to make the bandwidth of the CCC codes narrower allowing it to be well contained within the transducer's bandwidth. As an alternative approach, CCC can be used with Capacitive Micromachined Ultrasound Transducers (CMUT) which are a promising alternative to PZT transducers as they typically exhibit a large bandwidth with comparable and even improved sensitivity, enabling the transmission and reception of ultrasound waves over a broader range of frequencies [78], [79].

Additionally, simultaneously transmitting long sequences with all the elements of the probe may raise patient safety issues. The Mechanical Index (MI) and the Thermal Index (TI) are two metrics that regulate the safety limits of ultrasound systems. The MI is used to estimate potential bioeffects such as cavitation formation [80], and the TI is used as an indicator for possible tissue or probe damage caused by overheating [80], [81]. As stated in [82], the MI limit is often the dominating constraint when scanning the tissue with conventional focused beam. In our case, no focusing is performed which helps spreading the acoustic energy over the whole scanned tissue avoiding high peak pressures that can generate cavitation. The deriving voltage should also be decreased adequately with the length of the sequences to avoid temperature rise in both tissue and piezoelectric elements while keeping the thermal index at safe limits. This might of course reduce the theoretically achievable SNR improvement. Moreover, using low frequency probes can also help reducing the ultrasound absorption near the probe, hence limiting the tissue overheat in those areas, as well as using other probe technologies such as CMUTs which are less subject to heating.

Another aspect that needs to be considered is the decoding step of the RF signals. To obtain the full decoded STA dataset, the RF signals need to be correlated with each transmitted sequence. Because $(N, N, MN/P)$ -CCC have N sets of N sequences, N^2 correlations are required which can be time consuming for practical applications. In order to lessen the processing load of the decoding operation, instead of correlation in time domain, matrix multiplication is used in frequency domain by transforming the correlation operation into convolution operation, which reduces substantially the processing load of decoding. The optimization of the decoding process is considered in future works. In fact, with the $(N, N, MN/P)$ -CCC sequences used, during different transmit events, some elements may transmit the same sequence with only a sign change (+1 become a -1 and vice versa). This can be taken into advantage in order to reduce the number of correlations needed for the decoding by using simple addition and subtraction operations.

Finally, thanks to their ideal correlation properties and flexible code length, the use of CCC is not only restricted to sparse arrays, it can be applied to 1D arrays for 2D ultrasound imaging and also non-destructive testing application.

V. CONCLUSION

In this study, a CCC STA excitation scheme based on $(N, N, MN/P)$ -CCC has been proposed in order to increase the SNR of 2D sparse arrays with synthetic transmit aperture. Simulations using the Field II software were conducted to validate that CCC, usually used in a CDMA context, can be adapted to an ultrasound imaging problem. Compared to Conventional STA, the proposed CCC STA increases the SNR of spiral sparse array of around 41 dB and enhances the image contrast by almost 29 dB while maintaining the axial resolution and number of transmissions unchanged. Five other coded excitation schemes were compared to our method, enhancing again its ability preserve the axial resolution and frame rate. Future works will

include an experimental validation of the proposed CCC STA [83], [84], [85].

ACKNOWLEDGMENT

The authors would like to thank the members of the ANR SPARTECHUS Project for the suggestions and feedbacks on our work. A special thanks also to Jean-Baptiste Jacquet and Baptiste Piatol for the insightful discussions.

REFERENCES

- [1] O. Martínez-Graullera et al., "2D array design based on fermat spiral for ultrasound imaging," *Ultrasonics*, vol. 50, no. 2, pp. 280–289, Feb. 2010. [Online]. Available: <https://linkinghub.elsevier.com/retrieve/pii/S0041624X09001115>
- [2] A. Trucco, "Thinning and weighting of large planar arrays by simulated annealing," *IEEE Trans. Ultrasonics, Ferroelect. Freq. Control*, vol. 46, no. 2, pp. 347–355, Mar. 1999. [Online]. Available: <https://ieeexplore.ieee.org/document/753023/>
- [3] M. F. Rasmussen and J. A. Jensen, "3D ultrasound imaging performance of a row-column addressed 2D array transducer: A simulation study," in *Proc. IEEE Int. Ultrasonics Symp.*, 2013, pp. 1460–1463. [Online]. Available: <https://proceedings.spiedigitallibrary.org/proceeding.aspx?doi=10.1117/12.2007083>
- [4] M. F. Rasmussen et al., "3-D imaging using row-column-addressed arrays with integrated apodization - part I: Apodization design and line element beamforming," *IEEE Trans. Ultrasonics, Ferroelect., Freq. Control*, vol. 62, no. 5, pp. 947–958, May 2015. [Online]. Available: <https://ieeexplore.ieee.org/document/7103534/>
- [5] J. Hansen-Shearer et al., "Ultrafast 3-D ultrasound imaging using row-column array-specific frame-multiply-and-sum beamforming," *IEEE Trans. Ultrasonics, Ferroelect., Freq. Control*, vol. 69, no. 2, pp. 480–488, Feb. 2022. [Online]. Available: <https://ieeexplore.ieee.org/document/9591637/>
- [6] M. Flesch et al., "4D in VIVO ultrafast ultrasound imaging using a row-column addressed matrix and coherently-compounded orthogonal plane waves," *Phys. Med. Biol.*, vol. 62, no. 11, pp. 4571–4588, Jun. 2017. [Online]. Available: <https://iopscience.iop.org/article/10.1088/1361-6560/aa63d9>
- [7] L. T. Jorgensen et al., "Performance assessment of row-column transverse oscillation tensor velocity imaging using computational fluid dynamics simulation of carotid bifurcation flow," *IEEE Trans. Ultrasonics, Ferroelect., Freq. Control*, vol. 69, no. 4, pp. 1230–1242, Apr. 2022. [Online]. Available: <https://ieeexplore.ieee.org/document/9707796/>
- [8] J. Kortbek, J. A. Jensen, and K. L. Gammelmark, "Sequential beamforming for synthetic aperture imaging," *Ultrasonics*, vol. 53, no. 1, pp. 1–16, Jan. 2013. [Online]. Available: <https://linkinghub.elsevier.com/retrieve/pii/S0041624X12001138>
- [9] I. O. Wygant et al., "An integrated circuit with transmit beamforming flip-chip bonded to a 2-D CMUT array for 3-D ultrasound imaging," *IEEE Trans. Ultrasonics, Ferroelect., Freq. Control*, vol. 56, no. 10, pp. 2145–2156, Oct. 2009. [Online]. Available: <https://ieeexplore.ieee.org/document/5306761/>
- [10] G. Matrone et al., "A volumetric CMUT-based ultrasound imaging system simulator with integrated reception and -beamforming electronics models," *IEEE Trans. Ultrasonics, Ferroelect., Freq. Control*, vol. 61, no. 5, pp. 792–804, May 2014. [Online]. Available: <https://ieeexplore.ieee.org/document/6805693>
- [11] D. Bera et al., "Multiline 3D beamforming using micro-beamformed datasets for pediatric transesophageal echocardiography," *Phys. Med. Biol.*, vol. 63, no. 7, Mar. 2018, Art. no. 075015. [Online]. Available: <https://iopscience.iop.org/article/10.1088/1361-6560/aab45e>
- [12] B. Savord and R. Solomon, "Fully sampled matrix transducer for real time 3D ultrasonic imaging," in *Proc. IEEE Symp. Ultrason.*, 2003, pp. 945–953. [Online]. Available: <https://ieeexplore.ieee.org/document/1293556/>
- [13] C. Vallecilla and J. D'hooge, "Design of a multiplexing scheme for a matrix array for 3D cardiac imaging," in *Proc. IEEE Comput. Cardiol.*, 2016, pp. 877–879. [Online]. Available: <https://www.cinc.org/archives/2016/pdf/255-417.pdf>

- [14] T. L. Christiansen et al., "Row-column addressed 2-D CMUT arrays with integrated apodization," in *Proc. IEEE Int. Ultrasonics Symp.*, 2014, pp. 600–603. [Online]. Available: <https://ieeexplore.ieee.org/document/6931859/>
- [15] L. L. Wong et al., "A row-column addressed micromachined ultrasonic transducer array for surface scanning applications," *Ultrasonics*, vol. 54, no. 8, pp. 2072–2080, Dec. 2014. [Online]. Available: <https://linkinghub.elsevier.com/retrieve/pii/S0041624X14001929>
- [16] A. Ramalli et al., "Density-tapered spiral arrays for ultrasound 3-D imaging," *IEEE Trans. Ultrasonics, Ferroelect., Freq. Control*, vol. 62, no. 8, pp. 1580–1588, Aug. 2015. [Online]. Available: <https://ieeexplore.ieee.org/document/7185022/>
- [17] A. Ramalli et al., "Design, implementation, and medical applications of 2-D ultrasound sparse arrays," *IEEE Trans. Ultrasonics, Ferroelect., Freq. Control*, vol. 69, no. 10, pp. 2739–2755, Oct. 2022. [Online]. Available: <https://ieeexplore.ieee.org/document/9741756/>
- [18] Y. Li, M. C. Kolios, and Y. Xu, "3-D large-pitch synthetic transmit aperture imaging with a reduced number of measurement channels: A feasibility study," *IEEE Trans. Ultrasonics, Ferroelect., Freq. Control*, vol. 68, no. 5, pp. 1628–1640, May 2021. [Online]. Available: <https://ieeexplore.ieee.org/document/9286480/>
- [19] E. Roux et al., "2-D ultrasound sparse arrays multidepth radiation optimization using simulated annealing and spiral-array inspired energy functions," *IEEE Trans. Ultrasonics, Ferroelect., Freq. Control*, vol. 63, no. 12, pp. 2138–2149, Dec. 2016. [Online]. Available: <https://ieeexplore.ieee.org/document/7549037/>
- [20] E. Roux et al., "Experimental 3-D ultrasound imaging with 2-D sparse arrays using focused and diverging waves," *Sci. Rep.*, vol. 8, no. 1, Jun. 2018, Art. no. 9108. [Online]. Available: <https://www.nature.com/articles/s41598-018-27490-2>
- [21] D. H. Turnbull and F. S. Foster, "Beam steering with pulsed two-dimensional transducer arrays," *IEEE Trans. Ultrasonics, Ferroelect. Freq. Control*, vol. 38, no. 4, pp. 320–333, Jul. 1991. [Online]. Available: <https://ieeexplore.ieee.org/document/84270/>
- [22] J. L. Schwartz and B. D. Steinberg, "Ultrasparse, ultrawideband arrays," *IEEE Trans. Ultrasonics, Ferroelect. Freq. Control*, vol. 45, no. 2, pp. 376–393, Mar. 1998. [Online]. Available: <https://ieeexplore.ieee.org/document/660149/>
- [23] A. Austeng and S. Holm, "Sparse 2-D arrays for 3-D phased array imaging - design methods," *IEEE Trans. Ultrasonics, Ferroelect. Freq. Control*, vol. 49, no. 8, pp. 1073–1086, Aug. 2002. [Online]. Available: <https://ieeexplore.ieee.org/document/1026019/>
- [24] V. Murino, A. Trucco, and C. Regazzoni, "Synthesis of unequally spaced arrays by simulated annealing," *IEEE Trans. Signal Process.*, vol. 44, no. 1, pp. 119–122, Jan. 1996. [Online]. Available: <https://ieeexplore.ieee.org/document/482017/>
- [25] B. Diarra et al., "Design of optimal 2-D nongrid sparse arrays for medical ultrasound," *IEEE Trans. Biomed. Eng.*, vol. 60, no. 11, pp. 3093–3102, Nov. 2013. [Online]. Available: <https://ieeexplore.ieee.org/document/6529099/>
- [26] E. Roux et al., "Wideband 2-D array design optimization with fabrication constraints for 3-D US imaging," *IEEE Trans. Ultrasonics, Ferroelect., Freq. Control*, vol. 64, no. 1, pp. 108–125, Jan. 2017. [Online]. Available: <https://ieeexplore.ieee.org/document/7581110/>
- [27] C. Sciallero and A. Trucco, "Design of a sparse planar array for optimized 3D medical ultrasound imaging," in *Proc. IEEE 23rd Eur. Signal Process. Conf.*, 2015, pp. 1341–1345. [Online]. Available: <https://ieeexplore.ieee.org/document/7362602/>
- [28] C. Sciallero and A. Trucco, "Wideband 2-D sparse array optimization combined with multiline reception for real-time 3-D medical ultrasound," *Ultrasonics*, vol. 111, Mar. 2021, Art. no. 106318. [Online]. Available: <https://linkinghub.elsevier.com/retrieve/pii/S0041624X2030250X>
- [29] R. L. Haupt, "Thinned arrays using genetic algorithms," *IEEE Trans. Antennas Propag.*, vol. 42, no. 7, pp. 993–999, Jul. 1994.
- [30] P. K. Weber et al., "Optimization of random sparse 2-D transducer arrays for 3-D electronic beam steering and focusing," in *Proc. IEEE Ultrasonics Symp.*, 1994, pp. 1503–1506. [Online]. Available: <https://ieeexplore.ieee.org/document/401875/>
- [31] A. Austeng et al., "1D and 2D algorithmically optimized sparse arrays," in *Proc. IEEE Ultrasonics Int. Symp.*, 1997, pp. 1683–1686. [Online]. Available: <https://ieeexplore.ieee.org/document/663319/>
- [32] T. S. Sumanaweera, J. Schwartz, and D. Napolitano, "A spiral 2D phased array for 3D imaging," in *Proc. IEEE Ultrasonics Int. Symp.*, 1999, pp. 1271–1274. [Online]. Available: <https://ieeexplore.ieee.org/document/849228/>
- [33] M. C. Viganó et al., "Sunflower array antenna with adjustable density taper," *Int. J. Antennas Propag.*, vol. 2009, pp. 1–10, 2009. [Online]. Available: <https://www.hindawi.com/journals/ijap/2009/624035/>
- [34] H. Favre et al., "Boosting transducer matrix sensitivity for 3D large field ultrasound localization microscopy using a multi-lens diffracting layer: A simulation study," *Phys. Med. Biol.*, vol. 67, no. 8, Apr. 2022, Art. no. 085009. [Online]. Available: <https://iopscience.iop.org/article/10.1088/1361-6560/ac5f72>
- [35] J. R. Klauder et al., "The theory and design of chirp radars," *Bell System Tech. J.*, vol. 39, no. 4, pp. 745–808, Jul. 1960. [Online]. Available: <https://ieeexplore.ieee.org/document/6773600>
- [36] M. O'Donnell, "Coded excitation system for improving the penetration of real-time phased-array imaging systems," *IEEE Trans. Ultrasonics, Ferroelect. Freq. Control*, vol. 39, no. 3, pp. 341–351, May 1992. [Online]. Available: <https://ieeexplore.ieee.org/document/143168/>
- [37] T. X. Misaridis et al., "Potential of coded excitation in medical ultrasound imaging," *Ultrasonics*, vol. 38, no. 1-8, pp. 183–189, Mar. 2000. [Online]. Available: <https://linkinghub.elsevier.com/retrieve/pii/S0041624X99001304>
- [38] T. Misaridis and J. A. Jensen, "Use of modulated excitation signals in medical ultrasound. Part I: Basic concepts and expected benefits," *IEEE Trans. Ultrasonics, Ferroelect. Freq. Control*, vol. 52, no. 2, pp. 177–191, Feb. 2005. [Online]. Available: <https://ieeexplore.ieee.org/document/1406545/>
- [39] T. Misaridis and J. Jensen, "Use of modulated excitation signals in medical ultrasound. Part II: Design and performance for medical imaging applications," *IEEE Trans. Ultrasonics, Ferroelect. Freq. Control*, vol. 52, no. 2, pp. 192–207, Feb. 2005. [Online]. Available: <https://ieeexplore.ieee.org/document/1406546/>
- [40] T. Misaridis and J. A. Jensen, "Use of modulated excitation signals in medical ultrasound. Part III: High frame rate imaging," *IEEE Trans. Ultrasonics, Ferroelect. Freq. Control*, vol. 52, no. 2, pp. 208–219, Feb. 2005. [Online]. Available: <https://ieeexplore.ieee.org/document/1406547/>
- [41] K. L. Gammelmark and J. A. Jensen, "Multielement synthetic transmit aperture imaging using temporal encoding," *IEEE Trans. Med. Imag.*, vol. 22, no. 4, pp. 552–563, Apr. 2003. [Online]. Available: <https://ieeexplore.ieee.org/document/1200935/>
- [42] V. Behar and D. Adam, "Parameter optimization of pulse compression in ultrasound imaging systems with coded excitation," *Ultrasonics*, vol. 42, no. 10, pp. 1101–1109, Aug. 2004. [Online]. Available: <https://linkinghub.elsevier.com/retrieve/pii/S0041624X04001350>
- [43] V. Behar and D. Adam, "Optimization of sparse synthetic transmit aperture imaging with coded excitation and frequency division," *Ultrasonics*, vol. 43, no. 10, pp. 777–788, Dec. 2005. [Online]. Available: <https://linkinghub.elsevier.com/retrieve/pii/S0041624X0500048X>
- [44] A. Ramalli et al., "A real-time chirp-coded imaging system with tissue attenuation compensation," *Ultrasonics*, vol. 60, pp. 65–75, Jul. 2015. [Online]. Available: <https://linkinghub.elsevier.com/retrieve/pii/S0041624X15000463>
- [45] B. Pialot et al., "Sensitivity enhancement using chirp transmission for an ultrasound arthroscopic probe," *IEEE Trans. Ultrasonics, Ferroelect., Freq. Control*, vol. 69, no. 10, pp. 2776–2784, Oct. 2022. [Online]. Available: <https://ieeexplore.ieee.org/document/9738618/>
- [46] A. Nowicki et al., "On the application of signal compression using Golay's codes sequences in ultrasound diagnostic," *Arch. Acoust.*, vol. 28, pp. 313–324, 2003.
- [47] A. Nowicki et al., "Golay's codes sequences in ultrasonography."
- [48] C. Jin et al., "A new scheme of coded ultrasound using Golay codes," *J. Zhejiang Univ. Sci. C*, vol. 11, no. 6, pp. 476–480, Jun. 2010. [Online]. Available: <https://link.springer.com/10.1631/jzus.C0910353>
- [49] I. Trots et al., "Golay coded sequences in synthetic aperture imaging systems," *Arch. Acoust.*, vol. 36, no. 4, pp. 913–926, Jan. 2011. [Online]. Available: <https://journals.pan.pl/dlibra/publication/120028/edition/104452/content>
- [50] M. Yang and C. Chakrabarti, "Design of orthogonal coded excitation for synthetic aperture imaging in ultrasound systems," in *Proc. IEEE Int. Symp. Circuits Syst.*, 2012, pp. 113–116. [Online]. Available: <https://ieeexplore.ieee.org/document/6271430/>
- [51] D. Romero-Laorden et al., "Application of Golay codes to improve SNR in coarray based synthetic aperture imaging systems," in *Proc. IEEE 7th Sensor Array Multichannel Signal Process. Workshop*, Jun. 2012, pp. 325–328. [Online]. Available: <https://ieeexplore.ieee.org/document/6250501/>

- [52] R. Y. Chiao, L. J. Thomas, and S. D. Silverstein, "Sparse array imaging with spatially-encoded transmits," in *Proc. IEEE Ultrasonics Int. Symp.*, 1997, pp. 1679–1682. [Online]. Available: <https://ieeexplore.ieee.org/document/663318/>
- [53] P. Gong et al., "Delay-encoded transmission in synthetic transmit aperture (DE-STA) imaging," in *Proc. IEEE Int. Ultrasonics Symp.* 2014, pp. 1005–1008. [Online]. Available: <https://ieeexplore.ieee.org/document/6931894/>
- [54] P. Gong, M. C. Kolios, and Y. Xu, "Delay-encoded transmission and image reconstruction method in synthetic transmit aperture imaging," *IEEE Trans. Ultrasonics, Ferroelect., Freq. Control*, vol. 62, no. 10, pp. 1745–1756, Oct. 2015. [Online]. Available: <https://ieeexplore.ieee.org/document/7296563/>
- [55] Y. Wang et al., "Hadamard-encoded synthetic transmit aperture imaging for improved lateral motion estimation in ultrasound elastography," *IEEE Trans. Ultrasonics, Ferroelect., Freq. Control*, vol. 69, no. 4, pp. 1204–1218, Apr. 2022. [Online]. Available: <https://ieeexplore.ieee.org/document/9698091/>
- [56] E. Tiran et al., "Multiplane wave imaging increases signal-to-noise ratio in ultrafast ultrasound imaging," *Phys. Med. Biol.*, vol. 60, no. 21, pp. 8549–8566, Nov. 2015. [Online]. Available: <https://iopscience.iop.org/article/10.1088/0031-9155/60/21/8549>
- [57] Y. Zhang, Y. Guo, and W.-N. Lee, "Ultrafast ultrasound imaging with cascaded dual-polarity waves," *IEEE Trans. Med. Imag.*, vol. 37, no. 4, pp. 906–917, Apr. 2018. [Online]. Available: <https://ieeexplore.ieee.org/document/8170295/>
- [58] S. I. Nikolov, *Synthetic Aperture Tissue and flow Ultrasound Imaging*. Lyngby, Denmark: Tech. Univ. Denmark, 2002, Art. no. 334.
- [59] N. Suehiro and M. Hatori, "N-shift cross-orthogonal sequences," *IEEE Trans. Inf. Theory*, vol. 34, no. 1, pp. 143–146, Jan. 1988. [Online]. Available: <https://ieeexplore.ieee.org/document/2615/>
- [60] C.-C. Tseng and C. Liu, "Complementary sets of sequences," *IEEE Trans. Inf. Theory*, vol. 18, no. 5, pp. 644–652, Sep. 1972.
- [61] C. Han, N. Suehiro, and T. Imoto, "A generation method of length of MN complete complementary code," *IEICE Trans. Fundamentals*, vol. 88, no. 3, pp. 357–363, 2005.
- [62] C. Han and N. Suehiro, "A generation method for constructing (N,N,MN/P) complete complementary sequences," in *Proc. IEEE Joint 1st Workshop Mobile Future Symp. Trends Commun.*, 2004, pp. 70–73. [Online]. Available: <https://ieeexplore.ieee.org/document/1409501/>
- [63] M. Dávideková et al., "Applications of complete complementary codes and propositions for future research areas of these codes," *Procedia Comput. Sci.*, vol. 83, pp. 592–599, 2016. [Online]. Available: <https://linkinghub.elsevier.com/retrieve/pii/S187705091630312X>
- [64] H. H. Chen, J. F. Yeh, and N. Suehiro, "A multicarrier CDMA architecture based on orthogonal complementary codes for new generations of wide-band wireless communications," *IEEE Commun. Mag.*, vol. 39, no. 10, pp. 126–135, Oct. 2001. [Online]. Available: <https://ieeexplore.ieee.org/document/956124/>
- [65] N. Suehiro, "A signal design without co-channel interference for approximately synchronized CDMA systems," *IEEE J. Sel. Areas Commun.*, vol. 12, no. 5, pp. 837–841, Jun. 1994. [Online]. Available: <https://ieeexplore.ieee.org/document/298057/>
- [66] N. Suehiro and N. Kuroyanagi, "Binary signal design for approximately synchronized CDMA systems without detection sidelobe nor co-channel interference using auto- and cross-complementary codes," in *Proc. IEEE Int. Conf. Universal Pers. Commun. Conf.*, 1998, pp. 1097–1102. [Online]. Available: <https://ieeexplore.ieee.org/document/733672/>
- [67] C.-Y. Pai et al., "Designing two-dimensional complete complementary codes for omnidirectional transmission in massive MIMO systems," in *Proc. IEEE Int. Symp. Inf. Theory*, 2022, pp. 2285–2290.
- [68] S. Han, "A complete complementary coded MIMO system and its performance in multipath channels," *IEEE Wireless Commun. Lett.*, vol. 3, no. 2, pp. 181–184, Apr. 2014. [Online]. Available: <https://ieeexplore.ieee.org/document/6706233/>
- [69] J. Tang, Z. Ma, and C. Han, "The application of complete complementary codes in MIMO radar," in *Proc. IEEE Int. Waveform Diversity Des. Conf.*, 2012, pp. 271–276. [Online]. Available: <https://ieeexplore.ieee.org/document/7311297/>
- [70] J. Jensen, "FIELD: A program for simulating ultrasound systems," *Med. Biol. Eng. Comput.*, vol. 34, pp. 351–352, Jan. 1996.
- [71] J. Jensen and N. B. Svendsen, "Calculation of pressure fields from arbitrarily shaped, apodized, and excited ultrasound transducers," *IEEE Trans. Ultrasonics, Ferroelect. Freq. Control*, vol. 39, no. 2, pp. 262–267, Mar. 1992. [Online]. Available: <https://ieeexplore.ieee.org/document/139123/>
- [72] R. Y. Chiao and Xiaohui Hao, "Coded excitation for diagnostic ultrasound: A system developer's perspective," *IEEE Trans. Ultrason., Ferroelect., Freq. Control*, vol. 52, no. 2, pp. 160–170, Feb. 2005.
- [73] A. R. Brenner et al., "Improved resolution and dynamic range in medical ultrasonic imaging using depth-dependent mismatched filtering," in *Proc. IEEE Ultrasonics Int. Symp.*, 1997, pp. 1475–1480. [Online]. Available: <https://ieeexplore.ieee.org/document/661855/>
- [74] G. S. Jeng et al., "A novel pulse compression technique using inverse filtering in frequency domain," in *Proc. IEEE Ultrasonics Int. Symp.*, 2001, pp. 1535–1538. [Online]. Available: <https://ieeexplore.ieee.org/document/992012/>
- [75] T. X. Misaridis, M. H. Pedersen, and J. A. Jensen, "Clinical use and evaluation of coded excitation in B-mode images," in *Proc. IEEE Ultrasonics Int. Symp.*, 2000, pp. 1689–1693. [Online]. Available: <https://ieeexplore.ieee.org/document/921647/>
- [76] A. Nowicki et al., "Influence of the ultrasound transducer bandwidth on selection of the complementary Golay bit code length," *Ultrasonics*, vol. 47, no. 1–4, pp. 64–73, Dec. 2007. [Online]. Available: <https://linkinghub.elsevier.com/retrieve/pii/S0041624X07000698>
- [77] L. Wei et al., "Sparse 2-D PZT-on-PCB arrays with density tapering," *IEEE Trans. Ultrasonics, Ferroelect., Freq. Control*, vol. 69, no. 10, pp. 2798–2809, Oct. 2022.
- [78] O. Oralkan et al., "Experimental characterization of collapse-mode CMUT operation," *IEEE Trans. Ultrasonics, Ferroelect. Freq. Control*, vol. 53, no. 8, pp. 1513–1523, Aug. 2006. [Online]. Available: <https://ieeexplore.ieee.org/document/1665109/>
- [79] R. P. Zangabad et al., "Real-time coded excitation imaging using a CMUT-Based side looking array for intravascular ultrasound," *IEEE Trans. Ultrasonics, Ferroelect., Freq. Control*, vol. 68, no. 6, pp. 2048–2058, Jun. 2021. [Online]. Available: <https://ieeexplore.ieee.org/document/9336716/>
- [80] J. G. Abbott, "Rationale and derivation of MI and TI-A review," *Ultrasound Med. Biol.*, vol. 25, no. 3, pp. 431–441, Mar. 1999. [Online]. Available: <https://linkinghub.elsevier.com/retrieve/pii/S0301562998001720>
- [81] T. A. Bigelow et al., "The thermal index: Its strengths, weaknesses, and proposed improvements," *J. Ultrasound Med.*, vol. 30, no. 5, pp. 714–734, May 2011. [Online]. Available: <https://doi.wiley.com/10.7863/jum.2011.30.5.714>
- [82] P. Kaczowski, "Arbitrary waveform generation with the verasonics research ultrasound platform," Verasonics, Kirkland, WA, USA, Tech. Rep., 2016.
- [83] J. C. E. De Souza et al., "Design of ultrasonic synthetic aperture imaging systems based on a non-grid 2D sparse array," *Sensors*, vol. 21, no. 23, Nov. 2021, Art. no. 8001. [Online]. Available: <https://www.mdpi.com/1424-8220/21/23/8001>
- [84] M. Zubair and R. J. Dickinson, "3D synthetic aperture imaging with a therapeutic spherical random phased array for transcortical applications," *Phys. Med. Biol.*, vol. 66, no. 3, Feb. 2021, Art. no. 035024. [Online]. Available: <https://iopscience.iop.org/article/10.1088/1361-6560/abd0d0>
- [85] X. Li, A. Gachagan, and P. Murray, "Design of 2D sparse array transducers for anomaly detection in medical phantoms," *Sensors*, vol. 20, no. 18, Sep. 2020, Art. no. 5370. [Online]. Available: <https://www.mdpi.com/1424-8220/20/18/5370>